applied system innovation

MDPI

Article

Numerical Simulation and Development of a Continuous Microwave-Assisted Pilot Plant for Shelled Almond Processing

Luciano Mescia [1], Alessandro Leone [2], Claudio Maria Lamacchia [3], Angela Ferraris [3], Domenico Caggiano [3], Antonio Berardi [2,*] and Antonia Tamborrino [2]

[1] Department of Electrical and Information Engineering (DEI), Politecnico di Bari, Via E. Orabona 4, 70125 Bari, Italy; luciano.mescia@poliba.it
[2] Department of Soil, Plant and Food Science (DiSSPA), University of Bari Aldo Moro, Via Amendola 165/a, 70126 Bari, Italy; alessandro.leone@uniba.it (A.L.); antonia.tamborrino@uniba.it (A.T.)
[3] IAMAtek srl, Via Nicholas Green 13/A, Bari S. Spirito, 70127 Bari, Italy; claudio.lamacchia@iamatek.com (C.M.L.); angela.ferraris@iamatek.com (A.F.); domenico.caggiano@iamatek.com (D.C.)
* Correspondence: antonio.berardi@uniba.it

Abstract: This paper outlines the numerical modeling procedure aimed at defining the guidelines for the development of a continuous microwave-assisted pilot plant for shelled almond disinfestation, as an alternative to the use of chemicals. To this end, a 3D Multiphysics numerical tool involving both electromagnetic and thermal models was developed to predict the temperature and electric field profiles inside the microwave treatment chamber. Three different microwave sources arrangements were simulated and the accuracy of the model was verified under different residence times of almonds in the treatment chamber using the developed prototype. The modeling results demonstrated that the arrangement having five microwave sources, each delivering a maximum power of 1.5 kW and frequency of 2.45 GHz, ensures good heating uniformity. The obtained results proved that the model enables the accurate prediction of the temperature trend (root-mean-square error/RMSE = 0.82). A strong linear regression was detected for the standard deviation between the simulated and experimental data (linear regression, R^2 = 0.91). The very low COV value for the experimental temperature data demonstrated the heating uniformity as the treatment time changed. The developed model and the simulation strategy used may provide useful design guidance for microwave-assisted continuous plants for disinfestation, with a significant impact on the almond industry.

Keywords: microwave heating; 3D simulation; temperature distribution; pilot plant; continuous flow; almond disinfestation

Citation: Mescia, L.; Leone, A.; Lamacchia, C.M.; Ferraris, A.; Caggiano, D.; Berardi, A.; Tamborrino, A. Numerical Simulation and Development of a Continuous Microwave-Assisted Pilot Plant for Shelled Almond Processing. *Appl. Syst. Innov.* **2024**, *7*, 43. https://doi.org/10.3390/asi7030043

Academic Editor: Christos Douligeris

Received: 22 February 2024
Revised: 14 May 2024
Accepted: 21 May 2024
Published: 27 May 2024

1. Introduction

The almond (*Prunus dulcis*) is one of the most popular dried fruits consumed in many countries in the world. It is highly appreciated by consumers thanks to its composition in terms of macronutrients and micronutrients [1] and because its regular consumption has many beneficial effects for human health [2,3]. Almonds are widely used to produce almond milk, snacks and yogurt, as well as being widely used in the food industry and in the confectionery industry [1,4].

As often happens with nuts, legumes, cereals, and many other foodstuffs, during the production, storage and marketing steps, contamination with insects or pests is one of the biggest problems [5–9]. As reported in [10,11], the main pests of harvested almonds are the Indian meal moth (*Plodia interpunctella*), navel orangeworm (*Amyelois transitella*) and red flour beetle (*Tribolium castaneum*). The proliferation of these parasites contributes to quantitative and qualitative losses of the product as well as to the loss of competitiveness for the entire supply chain. Therefore, before almonds are marketed, post-harvest phytosanitary treatments are often required to control insect pests. Chemical and physical

methods are used for managing these issues. Thanks to the cost-effectiveness and ease of use, disinfestation via chemical methods such as fumigation with hydrogen phosphide and propylene oxide is widely used across the globe to prevent or treat insect and pest control. On the other hand, fumigants have hazardous effects on humans and the environment, they require skilled and certified professionals for their use, insects can develop resistance to fumigants, and a low dose of chemical fumigation may be ineffective for killing insects in the egg stage. Additionally, the increasing demand for organic foods, and several other economic and ecological reasons, hinder the commercial usage of fumigants [10–12].

As reported in [13], non-chemical methods such as cold storage, a controlled atmosphere and low pressure require lengthy exposure as well as high investment and management costs. In addition, thermal treatments with hot air are not very effective since the high resistance to heat transfer by conduction triggers a slow heat transfer rate in almonds; thus, lengthy treatments and high running costs result [14].

Considering these drawbacks, electromagnetic fields at microwave (MW) frequencies may provide a valuable alternative for post-harvest insect control in dried agricultural commodities. MW heating has no harmful residual products, it does not leave any chemical residue in the food, it reduces adverse effects on the environment, it kills insects, larvae, eggs and others and it affects the reproduction of the survivors [15–19]. Additional advantages of MW systems, in the context of industrial plants, include (i) operator safety, (ii) process automation, (iii) fast and efficient heating, (iv) a reduced footprint compared to traditional heating technologies, (v) preservation of the nutritional quality of the food and (vi) compliance with the international environmental rules and with the requirements of the Montreal Protocol [20]. Food processing and production plays a significant role in man-made global greenhouse gas emissions, contributing to about one-third of them. Microwave technology has proven to be efficient for reducing energy consumption and heating time as well as to enable a higher heating rate, thus demonstrating itself to be eco-friendly and able to reduce the carbon footprint [21,22].

Although MW heating can readily deliver energy to generate heat in the moist portion within foods, some factors as thickness, geometry and dielectric properties of the food, as well as the geometry of the treatment chamber, can affect the heating uniformity [23,24]. As a result, some changes in the chemical composition of the flavors (combined perception of compounds responsible for taste and aroma), color and texture, negatively affect the overall quality of the food. Additionally, issues related to pathogen/insect survival and microbial safety can arise [25].

The improvement in heating uniformity as well as the maximization of the energy coupling to the food are still research challenges since they mainly depend on the electromagnetic field distribution within the microwave treatment chamber and the dielectric properties of materials.

To overcome this problem, several solutions have been proposed, such as using the resonance phenomenon and using various microwave frequencies; however, adding a stirrer in the reactor is generally the most effective and has been employed widely in microwave continuous-flow reactors. In fact, the stirring systems improve the uniformity of heating [26,27].

To this end, the finite element method and numerical simulation can be useful tools for the optimization of food heating strategies [28–31].

The only scientific research in which microwaves were used to disinfest almonds is reported in [10]. In this study, the authors asserted that the MW thermal treatment of unshelled almonds could represent an alternative to chemical fumigation, balancing the complete killing of insects with minimal thermal impact on product quality. However, in this research, a domestic microwave oven with discontinuous flow was used and heating uniformity was not investigated.

The primary aim in this study is the development of a semi-industrial microwave (MW) prototype with continuous mass flow for almond processing, capable of handling a feed rate of at least 2 kg min^{-1}, maintaining a minimal residence time of at least 90 s, and

achieving almond temperatures of up to 60 °C with homogeneous temperature distribution inside the treatment chamber. Moreover, numerical simulations were carried out with the main aim to identify the best design solution of the MW prototype (number of MW sources along the treatment chamber), ensuring an optimal heating uniformity during the whole process.

2. Materials and Methods

The sequential steps to study and develop the MW machine are listed below:

1. Study of the dielectric properties of unshelled almonds (*Prunus dulcis*). Filippo Ceo almonds variety was used. They were harvested in Toritto (BA-Italy) in August 2022, then hulled, dried, and shelled.
2. Development of a numerical model to define the minimum optimal number of magnetrons necessary to achieve the dual objective: (i) obtain uniformity of the magnetic field inside the treatment chamber along its entire length; (ii) ensure that the maximum temperature of at least 60 °C is reached with a residence time of no less than 90 s. Therefore, the numerical simulation was carried out without considering the movement of the almonds along the treatment chamber, as it did not influence the two pre-established objectives.
3. The placement of the MW sources feeding the treatment chamber of the prototype. In this regard, a 3D model coupling the electromagnetic and heat transfer processes was established using a multiphysics solver [32–34]. The temperature and electric field distribution inside the treatment chamber were analyzed under three different placements of the MW sources and at different processing times. The whole design was carried out taking care to prevent and minimize possible microwave energy leakage. To this end, honeycomb filters integrated in both loading and unloading sections of the pilot plant were suitably designed. In this way, the hazards due to the worker's exposure to microwaves were practically negligible, and the whole plant was compliant with international recommendations [35], European regulations [36] and Italian regulations limiting the exposure of people to electromagnetic fields [37].
4. Build of the semi-industrial MW-based pilot plant with continuous flow by means the internal helix.
5. Experimental trials with the aim of testing plant performance, and evaluating the temperature reached and the heating uniformity of processed almonds at different processing times. To this regard, the temperature values predicted with the numerical simulations were compared with the experimental results and statistically analyzed.

It should be noted that the numerical simulation was carried out statically (without a helix in the treatment chamber) while the experimental evaluations were carried out dynamically (with a helix in treatment chamber). Therefore while for the statistical comparison between the simulated and experimented temperatures the helix has no influence, since the temperature depends only on the generated magnetic field, for the uniformity of heating the helix can have an influence. These aspects were interpreted and reported in the results chapter.

2.1. Microwave Heating

The microwave heating of food is a complex multiphysics phenomenon involving electromagnetic fields in a cavity [38] and heat transfer. The interaction of MW energy with the charges and dipoles inside the food generates their translation or rotation. The resistance to this movement creates friction and collisions, which result in the transformation of MW energy into thermal energy. So, the MW heating process mainly depends on (i) the MW frequency (commonly 915 MHz and 2.45 GHz), (ii) the electromagnetic field pattern inside the treatment chamber, (iii) the dielectric properties of the food, and (iv) the heat dissipation due to the heat and mass transfer. Generally, it is difficult to examine the temperature profile and electromagnetic field distribution inside the closed metallic MW treatment

chamber during an actual thermal processing. Thus, it could be useful to predict such behaviors through a computer-based analysis.

2.2. Dielectric Properties

The effectiveness of MW heating can be quantified if the dielectric properties of the food are known. They can be assessed according to the complex relative permittivity defined by the equation

$$\varepsilon_r = \varepsilon_r{}' - j\varepsilon_r{}'' \quad (1)$$

where the dielectric constant $\varepsilon_r{}'$ and the dielectric loss factor $\varepsilon_r{}''$ quantify the capability of the material to store and dissipate MW energy, respectively. Several studies pertaining to the dielectric properties of many foods, such as fruits and vegetables, meat and ham, starch and glucose solutions, various food proteins and some types of pasta, have been published [23,39,40]. However, there are less data on the dielectric properties of almonds. On the other hand, the development of equations to predict the dielectric properties of food would be very useful to gain insights into interactions between food and electromagnetic energy. Within this framework, we used literature data and empirical equation modeling of both the dielectric constant and loss factor versus the temperature T and moisture content M [41]

$$\begin{aligned}\varepsilon_r{}' = 2.96 - 0.10T + 0.05M + 6.56 \times 10^{-3}TM + 2.41 \times 10^{-3}T^2 - 0.07M^2 - 2.31 \times 10^{-4}T^2M + 6.37 \times 10^{-4}TM^2 - \\ 1.65 \times 10^{-5}T^3 + 0.01M^3 + 3.72 \times 10^{-6}T^2M^2 + 8.94 \times 10^{-7}T^3M - 2.79 \times 10^{-5}TM^3 + 3.79 \times 10^{-8}T^4 - 3.12 \times 10^{-4}M^4\end{aligned} \quad (2)$$

and

$$\begin{aligned}\varepsilon_r{}'' = 11.54 - 0.09T - 4.95M + 0.01TM + 1.65 \times 10^{-3}T^2 - 0.72M^2 - 1.58 \times 10^{-4}T^2M - 5.29 \times 10^{-4}TM^2 \\ -1.35 \times 10^{-5}T^3 - 0.04M^3 + 3.36 \times 10^{-6}T^2M^2 + 6.00 \times 10^{-7}T^3M + 7.66 \times 10^{-6}TM^3 \\ +4.12 \times 10^{-8}T^4 + 8.36 \times 10^{-4}M^4\end{aligned} \quad (3)$$

Equations (2) and (3) refer to a frequency of 2.45 GHz; T and M can change from 20 to 90 °C and from 4.2% to 19.6%, respectively. Nevertheless, the food to be heated is generally a heterogeneous dielectric mixture consisting, in this case, of almonds embedded in a host material (air). Thus, to simplify the resulting complex and difficult electromagnetic problem we assumed a continuous effective medium having dielectric permittivity, given by

$$\varepsilon_{r,\,eff} = f_{al}\varepsilon_{r,\,al} + (1 - f_{al})\varepsilon_{r,air} \quad (4)$$

where $\varepsilon_{r,al}$, f_{al} and $\varepsilon_{r,air}$ are the relative dielectric permittivity of almonds, given by Equations (2) and (3), the volumetric concentration of almonds and the relative dielectric permittivity of air, respectively.

2.3. Electromagnetic and Thermal Modeling

The numerical modeling combines all relevant physics, including the electromagnetic interaction with the almond and plant components as well as the conductive and convective heat transfer. The electromagnetic energy distribution in the 3D space and over time was calculated by solving the time-domain integral form of the Maxwell equations [42]:

$$\oint_l E \cdot dl = -\int_S \frac{\delta B}{\delta t} \cdot \delta S \quad (5)$$

$$\oint_l B \cdot dl = \int_S \left(\frac{\delta D}{\delta t} + J\right) \cdot \delta S \quad (6)$$

$$\oint_S D \cdot dS = \int_V \rho dV \quad (7)$$

$$\oint_S B \cdot dS = 0 \quad (8)$$

in conjunction with the impedance and perfectly matched layer boundary conditions, as well as the relative permittivity of the materials present in the whole plant. In the calculations, all materials are non-magnetic; thus, their interaction with the magnetic field is negligible. The internal volumetric heat generation term, quantifying the power dissipated inside the material, can be evaluated using the equation

$$Q_{MW} = \pi f \varepsilon_0 \varepsilon''_{r,eff} |E|^2 \quad (9)$$

where f is the frequency of the MW signal, ε_0 is the vacuum permittivity, $\varepsilon''_{r,eff}$ is the effective dielectric loss factor, and E is the electric field. Once Q_{MW} is evaluated, the temperature distribution of food was calculated by solving the Fourier energy balance equation [43,44]:

$$\rho C_P \frac{\delta T}{\delta t} = \nabla \cdot (k \nabla T) + Q_{MW} \quad (10)$$

where C_P (Jkg^{-1}K^{-1}) is the specific heat, k (Wm^{-1}K^{-1}) is the thermal conductivity, ρ (kgm^{-3}) is the material density and T (K) is the temperature field. The energy balance equation is solved considering that the thermal properties of the food remain constant through the entire heating process and that the phase change, mass transfer and chemical reaction are negligible.

2.4. Numerical Modeling

The footprint of MW machine was chosen to develop a prototype that processed the product continuously; therefore, it was necessary to design a system consisting of a cylindrical treatment chamber and an internal transport system made up of a metallic helix. The design choice of using the helix as an alternative to the screw is due to its lower resistance to the diffusion of the microwaves in the volume of the treatment chamber.

The choices of the geometric parameters of the treatment chamber (diameter and length) arise from the operational needs of the system.

A minimum flow rate of the system equal to at least 2 kg min^{-1} and a minimal residence time of the almonds inside the treatment chamber equal to at least 90 s were assumed.

The flow rate and residence time values were measured on the basis of preliminary tests carried out before the construction of the plant, with a simplified prototype consisting of a feeding hopper, tube (treatment chamber) and internal helix (transport system).

Figure 1 shows the technical design of the MW prototype. The treatment chamber consists of a polypropylene tube (green region) with an inner diameter, outer diameter and length of the tube of 90.8 mm, 125 mm, and 3000 mm, respectively. Inside the tube a rotating metallic helix allows the almonds to be mixed and moved from the supply section to the discharge section. On the feeding side is placed a honeycomb filter integrated with the feed hopper. The dust extraction chamber is shown on the opposite side. Figure 1 shows three different setups with 1, 3 and 5 MW sources equidistant from each other along the treatment chamber:

A1: 1 MW source of 7.5 kW (Figure 1a);

A2: 3 MW sources of 2.5 kW (Figure 1b);

A3: 5 MW sources of 1.5 kW (Figure 1c).

For the three different arrangements, the numerical simulations were carried out under different processing times (residence time of the almonds inside the treatment tube) to identify the right number, placement, and MW power minimizing hotspots and allowing a uniform heating of the almonds in the treatment chamber. The residence time used for numerical simulation was of 80 s, 100 s, 120 s, 140 s, 160 s, 180 s and 200 s.

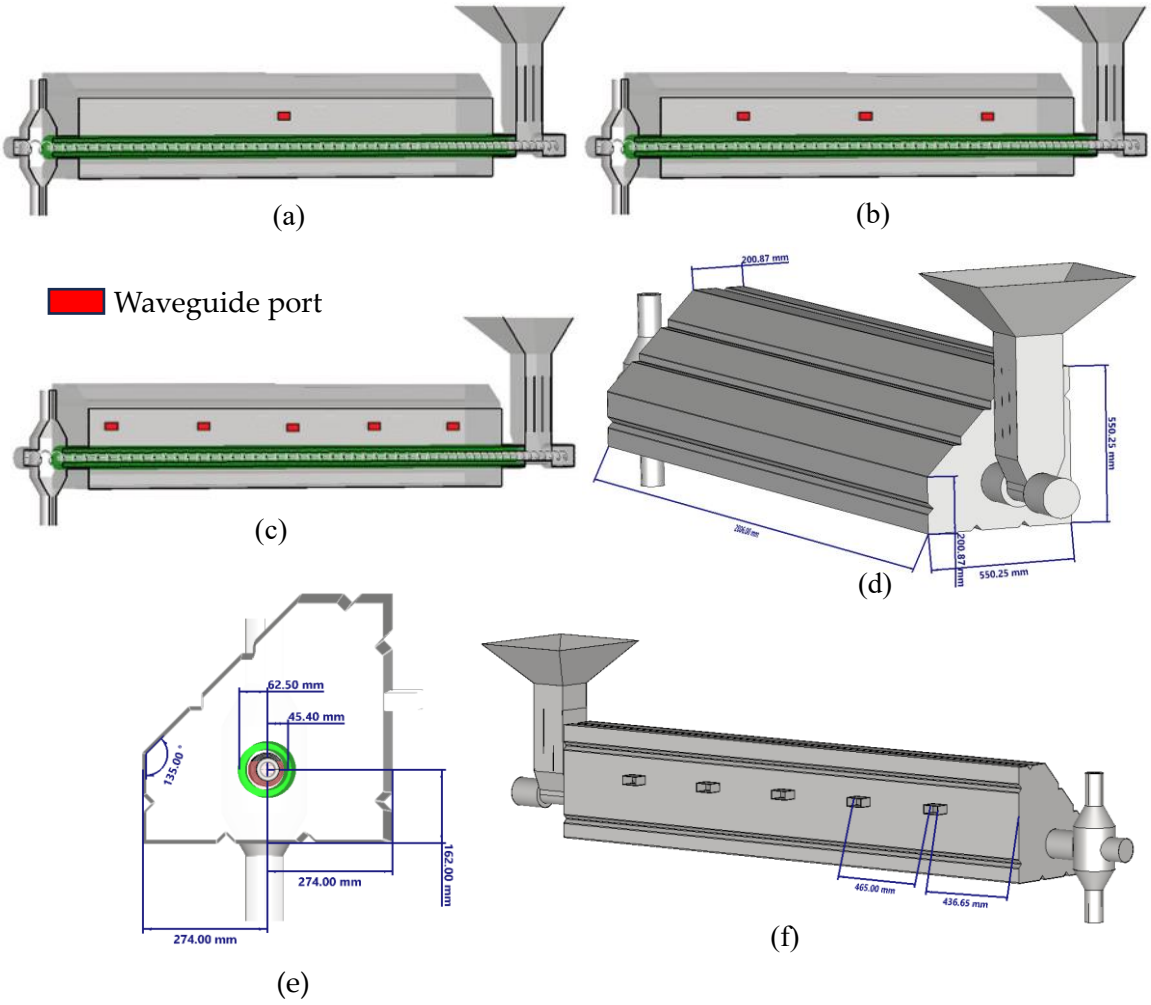

Figure 1. Technical design of the MW prototype arranged with (**a**) one, (**b**) two and (**c**) three microwave sources; (**d**) schematic of the microwave applicator on a perspective view; (**e**) schematic of the microwave applicator on a lateral view; (**f**) source location of the microwave applicator.

For each arrangement, the whole design was numerically carried out using the 3D simulation software Dassault Systemes CST STUDIO SUITE® 2022. The time domain solver was used to perform both the electromagnetic and thermal analyses. The computational domain is an air box containing the MW prototype. In this way, it was possible to quantify the electromagnetic field inside the treatment chamber as well as the one escaping in the external environment. So, the electromagnetic simulations were carried out considering a frequency range of 2.4 to 2.5 GHz and the perfectly matched layer boundary condition surrounding the whole computational domain. The waveguide port setting provided by the electromagnetic solver was used to feed the computational domain with power and to absorb the returning power. Hexahedral meshing was used, characterized by 10 cells per wavelength, 20 cells per max model box edge and a fraction of maximum cell near to model of 15 (giving about 30 million of cells). The thermal simulations were performed by fixing a temperature T_b = 16 °C on the boundary of the air box containing the MW prototype as well as a uniform initial temperature T_0 = 16 °C on the whole computational domain. The latter constrain is justified by considering the stationary solution of Equation (10) with no volumetric heat source. Moreover, Equation (10) was applied to the whole computational domain including the bunch of almonds, propylene tube, air volume inside and outside the treatment chamber, metallic walls and helix. Hexahedral meshing characterized by 30 cells per max model box edge and a fraction of maximum cell near to model of 20 (giving about 140,000 cells) was set. The accuracy was set at −40 dB and the high-order

method with adaptive time step was used for the time integration settings. The metal of the MW plant was modeled as a lossy 1010 stainless steel with an electric conductivity $\sigma = 7 \times 10^6$ Sm^{-1} according to Equations (2)–(4). The dielectric properties of almonds were calculated using Equations (2) and (3) by setting $M = 4.2\%$ and $T = T_b$. The resulting values were $\varepsilon'_{r,al} = 1.42$ and $\tan \delta = \varepsilon''_{r,al} / \varepsilon'_{r,al} = 0.14$. Moreover, the effective dielectric permittivity of the medium filling the polypropylene tube was calculated using Equation (4) by setting $f_{al} = 64\%$. However, the numerical simulations were carried out neglecting the movement of the almonds along the treatment chamber as well as by considering the honeycomb filter without almonds.

Table 1 summarizes the model parameters required to perform simulations.

Table 1. Electrical, thermal and geometrical parameters.

Symbol	Value	Description
f_0	2.45 GHz	Microwave frequency
$\varepsilon'_{r,al}$	1.42	Dielectric constant of almonds
$\tan \delta$	0.14	Dielectric loss factor of almonds
$\varepsilon'_{r,pl}$	2.30	Dielectric constant of polypropylene
$\tan \delta_{pl}$	0.002	Dielectric loss factor of polypropylene
σ	7×10^6 Sm^{-1}	Electric conductivity of stainless steel
k_a	0.1 Wm^{-1}K^{-1}	Thermal conductivity of almonds
k_p	0.24 Wm^{-1}K^{-1}	Thermal conductivity of polypropylene tube
k_s	65.2 Wm^{-1}K^{-1}	Thermal conductivity of stainless steel
C_{pa}	1400 Jkg^{-1}K^{-1}	Specific heat of almonds
C_{pp}	1000 Jkg^{-1}K^{-1}	Specific heat of polypropylene tube
C_{ps}	450 Jkg^{-1}K^{-1}	Specific heat of stainless steel
ρ_a	800 kgm^{-3}	Mass density of almonds
ρ_p	2200 kgm^{-3}	Mass density of polypropylene tube
ρ_s	7870 kgm^{-3}	Mass density of stainless steel
d_0	125 mm	Outer diameter of the propylene tube
d_i	90.8 mm	Inner diameter of the propylene tube
L_f	395 mm	Length of the honeycomb filter
W_f	180 mm	Width of the honeycomb filter
H_f	552 mm	Height of the honeycomb filter
W_g	60 mm	Width of the grid honeycomb filter
H_g	60 mm	Height of the grid honeycomb filter
L	3000 mm	Length of the treatment chamber
W	564 mm	Width of the treatment chamber
H	552 mm	Height of the treatment chamber

The simulated temperature field pertaining to the 3D space filled with almonds was sampled at 971 points along the longitudinal axis of the treatment chamber (step 3.14 mm) and 9 points on the transversal section; thus, 8739 samples were considered. Given that the inner cross section of the tube is a circle with the diameter d = 90.8 mm, the 9 points were chosen so that one corresponds to the center of the cross section (center), four to the diametrically opposed points on the concentric ring with the diameter $d_1 = 40.3$ mm (inner) and four on the concentric ring with the diameter $d_1 = 90.6$ mm (outer). Moreover, the same sampling was carried out for the following residence times: 80 s, 100 s, 120 s, 140 s, 160 s, 180 s and 200 s. Numerical simulations were performed using a workstation with two processors: Intel Xeon Gold, 3 GHz, 12 cores and RAM 512 GB, 266 MHz ECC.

2.5. Experimental Procedure to Evaluate the Thermal Uniformity

Following the results obtained with the numerical simulation, the MW prototype was built and tested to check its correct operation.

Almonds (*Prunus dulcis*) of the Tuono cultivar were used for the experimental tests. The harvested almonds were hulled, sun-dried, shelled and then stored at a controlled temperature of 18 °C.

Experimental test plans were carried out to measure the surface temperature of the outgoing almonds at residence times of 80 s, 100 s, 120 s, 140 s, 160 s, 180 s and 200 s, obtained by adjusting the electric motor frequency drive of the helix in the range between 30 Hz and 80 Hz. The measurement of the temperature of the almonds in the different test conditions was carried out using an infrared thermometer (Omega Engineering, mod. OM051-LT, Norwalk, CT, USA) installed at the exit of the treatment chamber. The data detected by the thermometer were reported on the control PLC of the MW plant.

Total MW power was 7.5 kW. The almonds used for the experiments had been previously stored and kept at a constant temperature of 16 °C (the same initial temperature assumed for the numerical simulation) in a temperature-controlled chamber. For each trial, a homogeneous batch of almonds of 150 kg was used. Each trial was repeated 10 times.

During trials, the flow rate was determined by measuring the time needed to treat the 150 kg batch of almonds; in addition, the surface temperature of the almonds at the end of the treatment was determined using a thermal imager (Testo 876, Testo SE & Co. KGaA, Lenzkirch, Germany) with uncertainty of ±2%, an FPA 160 × 120 pixel, a range measurement spectrum from 8 up to 14 µm and an update frequency of 9 Hz. The thermal pictures were captured at 0.5 m. Thirty thermal images were processed for each test condition.

2.6. Moisture Content of Almonds

The moisture content of the shelled almonds (% wet basis) was detected according to the method described in [45], both on samples of untreated and microwave-treated almonds.

2.7. Statistical Analysis

MATLAB® (The Mathworks Inc., Natick, MA, USA) machine learning and statistical toolboxes were used for the experimental data processing. Significance set at $p < 0.05$ was tested using ANOVA and the Tukey–Kramer test for mean separation.

The coefficient of variation (*COV*) is expressed as

$$COV = \frac{1}{T_a - T_0}\sqrt{\frac{\sum_{i=1}^{N}(T_i - T_a)^2}{N}} \quad (11)$$

and was used to describe the uniform temperature distribution [31] both for the simulated and experimental temperatures. In Equation (11), T_i and T_a are, respectively the mesh point and average temperature after microwave heating, T_o is the initial average temperature and N is the number of mesh points.

To verify the uniformity of the surface temperature of the almonds coming out after the MW treatment in the simulation model, the *COV* was calculated considering 19,200 mesh points (matrix from 160 to 120) of each thermal image.

The root-mean-square error (*RMSE*) is expressed as

$$RMSE = \sqrt{\frac{\sum_{i=1}^{N}(T_i - T_a)^2}{N}} \quad (12)$$

and was used to measure the error of the model in predicting of the temperature [29,30].

3. Results and Discussion

3.1. Simulation Results

Figures 2a, 3a and 4a show the 2D electric field intensity profiles corresponding to arrangement 1, arrangement 2 and arrangement 3, respectively. In all three arrangements a very good electric field confinement inside the treatment chamber was obtained. Moreover, it can be inferred that the honeycomb filters effectively shield the electromagnetic field from escaping into the external environment. The corresponding temperature profiles at residence

times of 80 s, 140 s and 200 s are shown in Figures 2b–d, 3b–d and 4b–d, too. Arrangements 1 and 2 exhibit a non-uniform temperature distribution having hot spots located in the regions of space close to the sections where the microwave power is started within the treatment chamber. Furthermore, the thermal non-uniformity increases as the residence time increases. On the other hand, arrangement 3 ensures a quite uniform temperature distribution inside the polypropylene tube filled with almonds even for long treatment times.

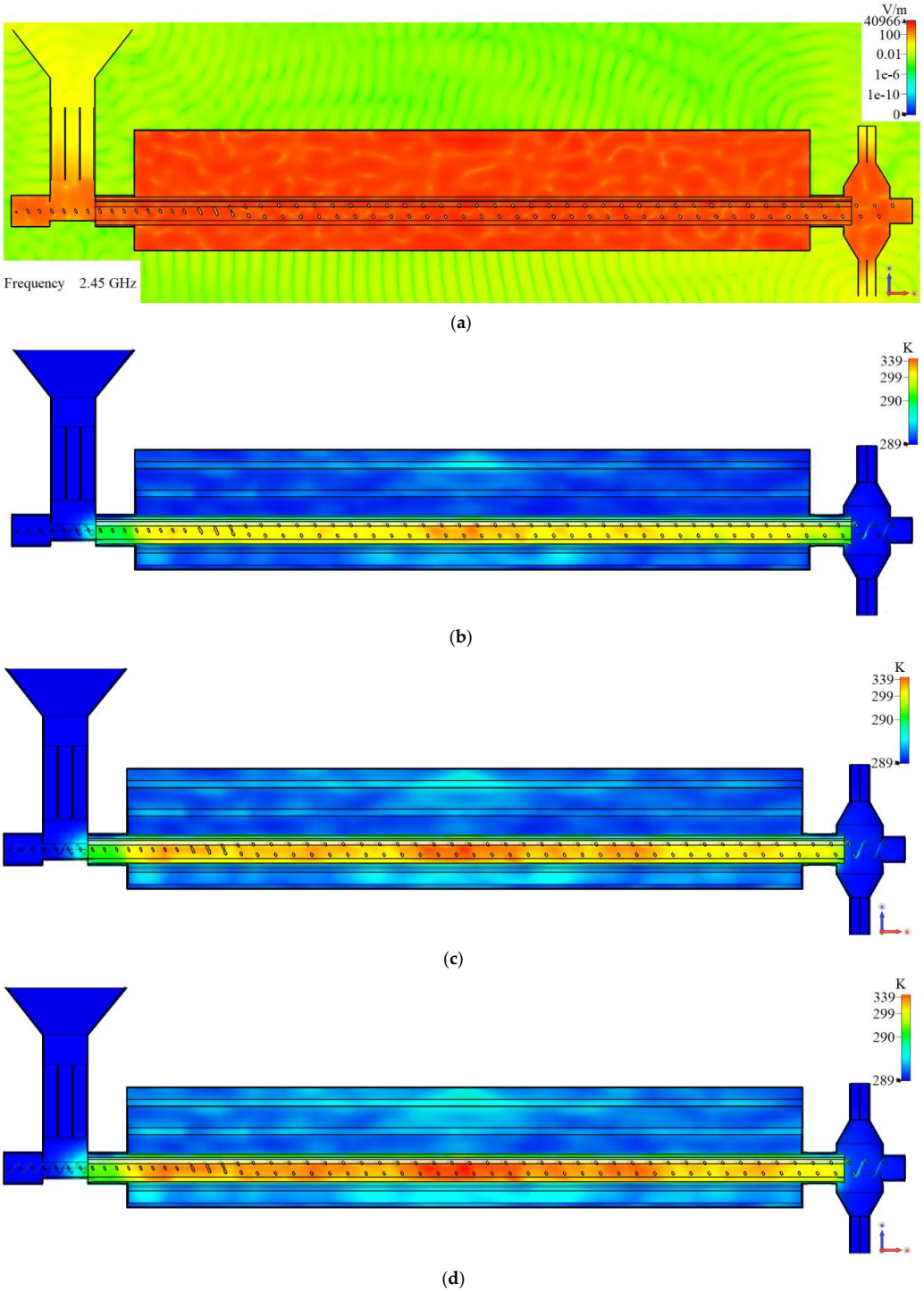

Figure 2. (**a**) Numerical simulation of electric field and temperature distributions after (**b**) 80 s, (**c**) 140 s, and (**d**) 200 s for arrangement 1. Frequency f = 2.45 GHz and total MW power P_T = 7.5 kW.

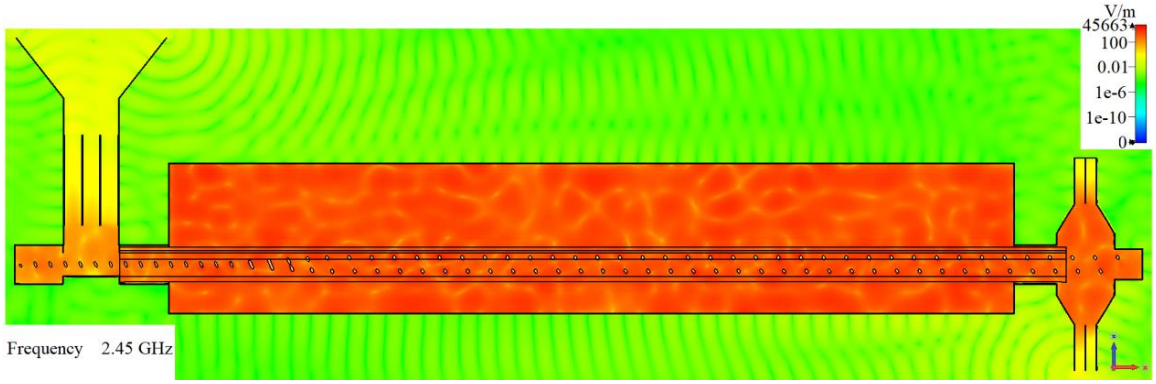

(**a**)

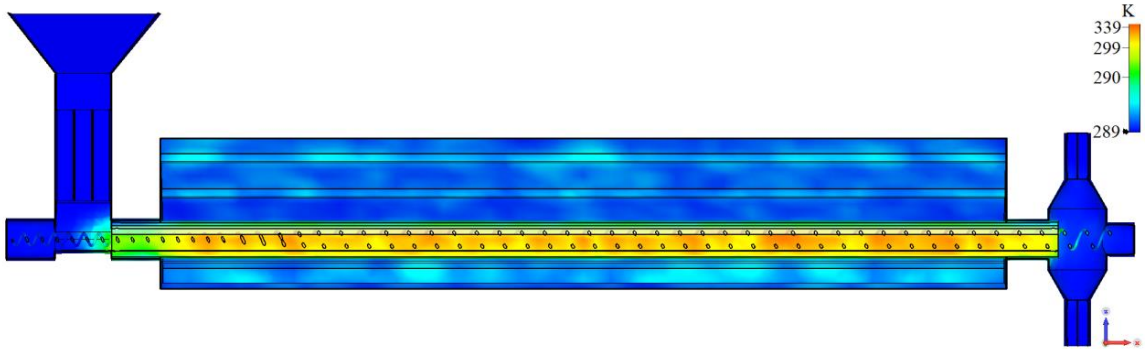

(**b**)

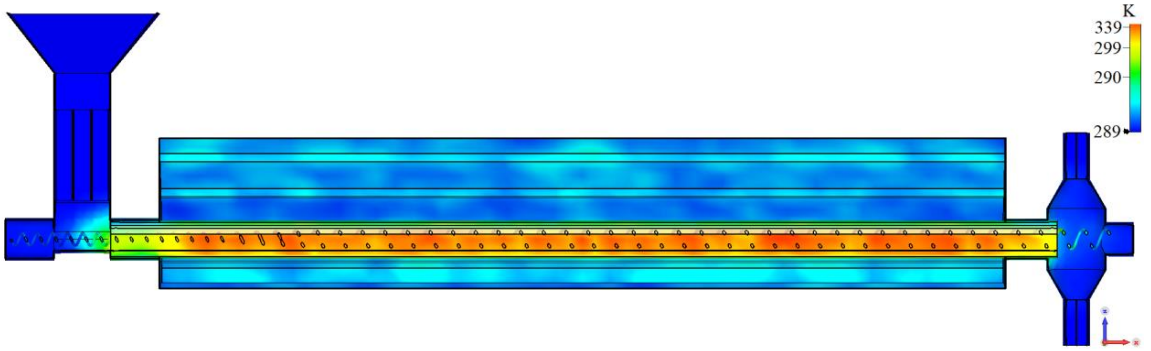

(**c**)

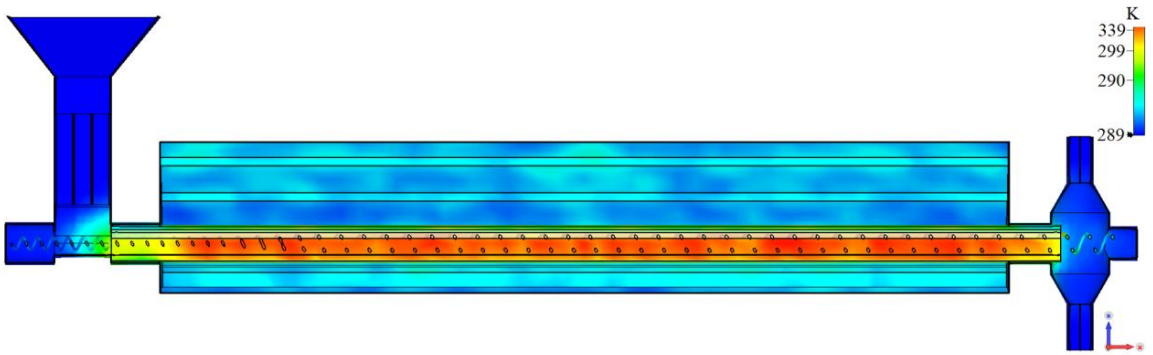

(**d**)

Figure 3. (**a**) Numerical simulation of electric field and temperature distributions after (**b**) 80 s, (**c**) 140 s, and (**d**) 200 s for arrangement 2. Frequency f = 2.45 GHz and total MW power P_T = 7.5 kW.

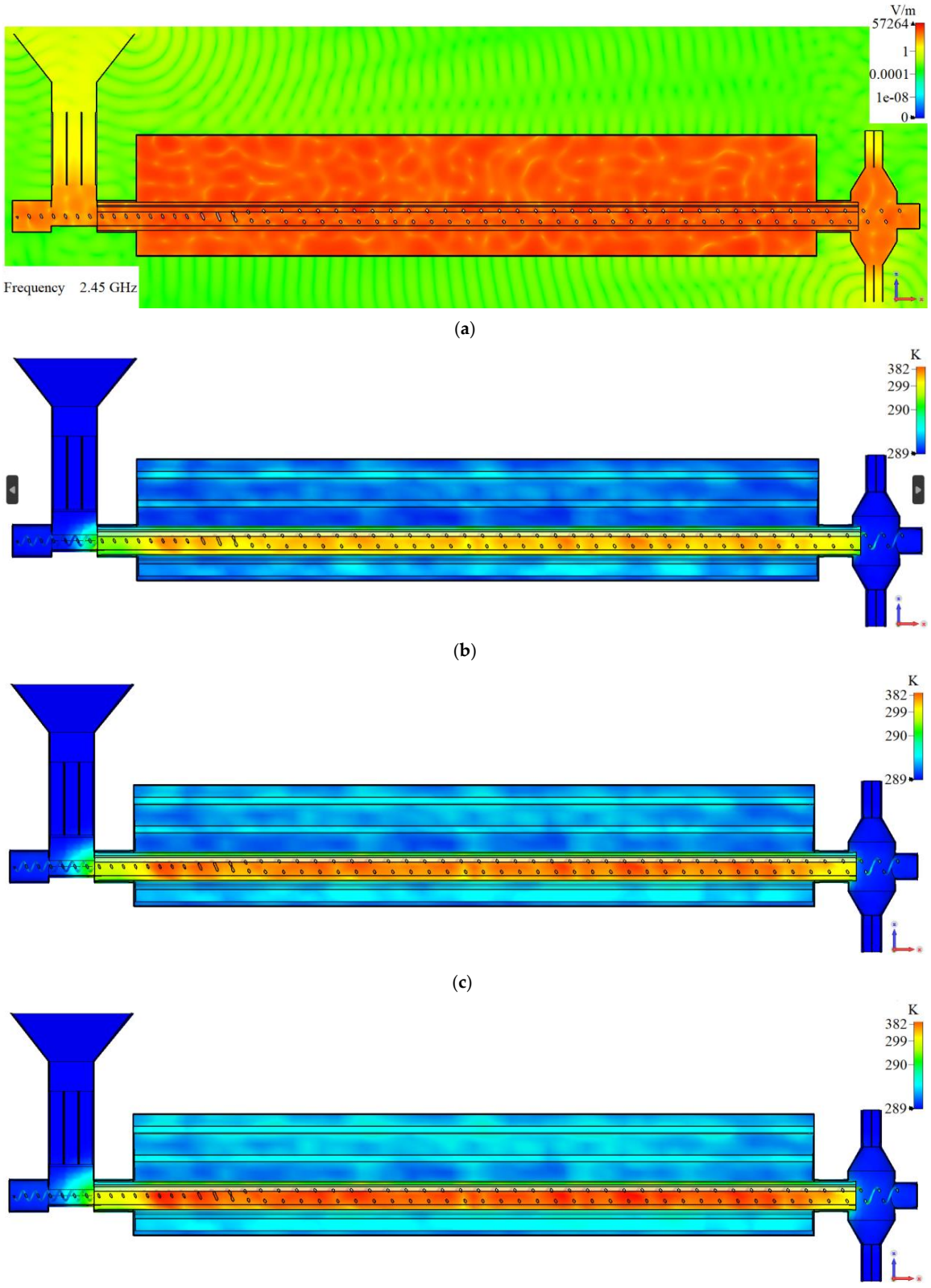

Figure 4. (**a**) Numerical simulation of electric field and temperature distributions after (**b**) 80 s, (**c**) 140 s, and (**d**) 200 s for arrangement 3. Frequency f = 2.45 GHz and total MW power P_T = 7.5 kW.

Considering that the simulations refer to multiport feeding, the design was carried out with the aim to maximize the overall system efficiency. To this aim, the incoming and outcoming microwave powers pertaining to the five active ports of the A3 set up are reported in Table 2. It is worth noting that with respect to the total power released by magnetrons (7.5 kW), about 7 kW came into the microwave applicator, thus ensuring an efficiency of about 93%.

Table 2. Microwave power pertaining to each waveguide port of the A3 set up.

	Incoming Power (W)	Outcoming Power (W)
Port 1	1419.60	80.40
Port 2	1358.23	141.77
Port 3	1403.45	96.55
Port 4	1395.64	104.36
Port 5	1382.40	117.60
TOTAL	6959.33	540.67

To evaluate the uniformity of MW heating, numerical data were post-processed. A first temperature data processing step of the treatment tube cross section was carried out as follows: (1) grouping the temperature data along the longitudinal direction in the center of the cross section, (2) grouping the temperature data along the longitudinal direction of the inner ring with diameter d_1 = 40.3 mm, and (3) grouping the temperature data along the longitudinal direction of the outer ring diameter d_2 = 90.6 mm.

The data obtained show that for all arrangements at any residence time of the almonds in the treatment chamber between 80 and 200 s, there were no significant differences in the simulated temperature in the center, inner and outer sections. Simulation results for the mean temperature, standard deviation and the COV and pertaining the different arrangements are shown in Figure 5.

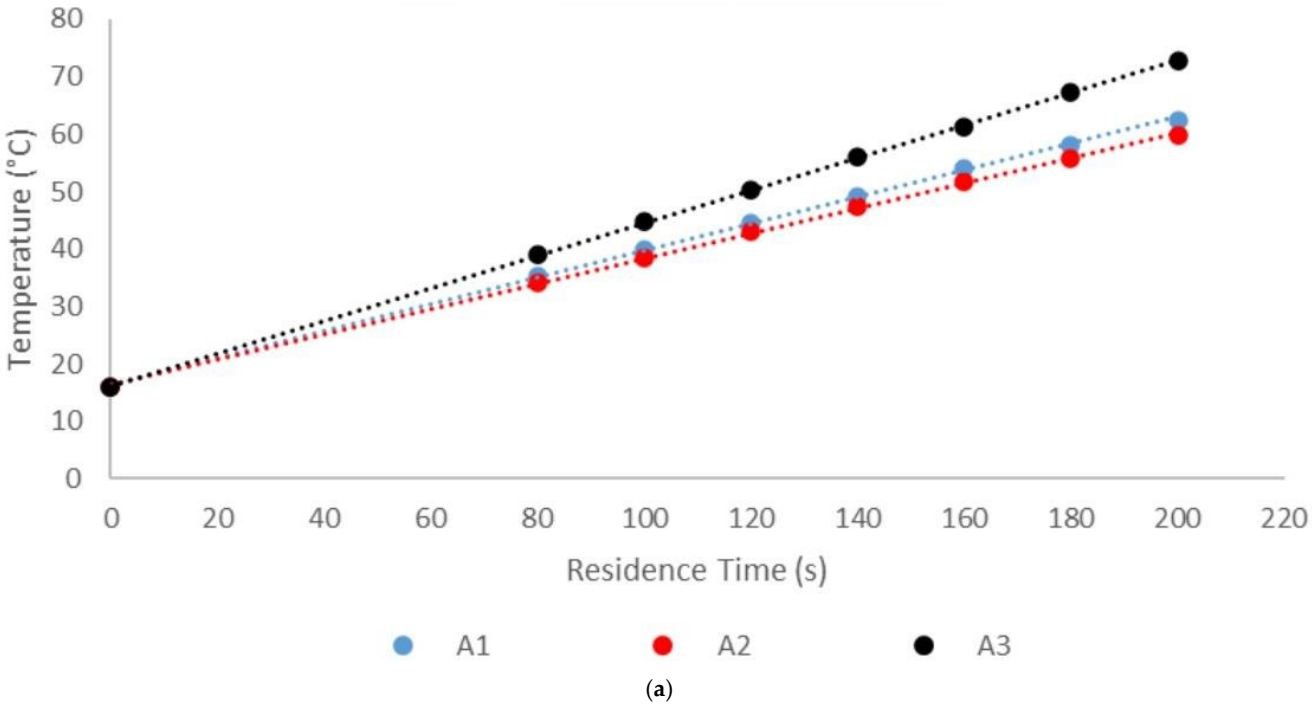

(**a**)

Figure 5. *Cont.*

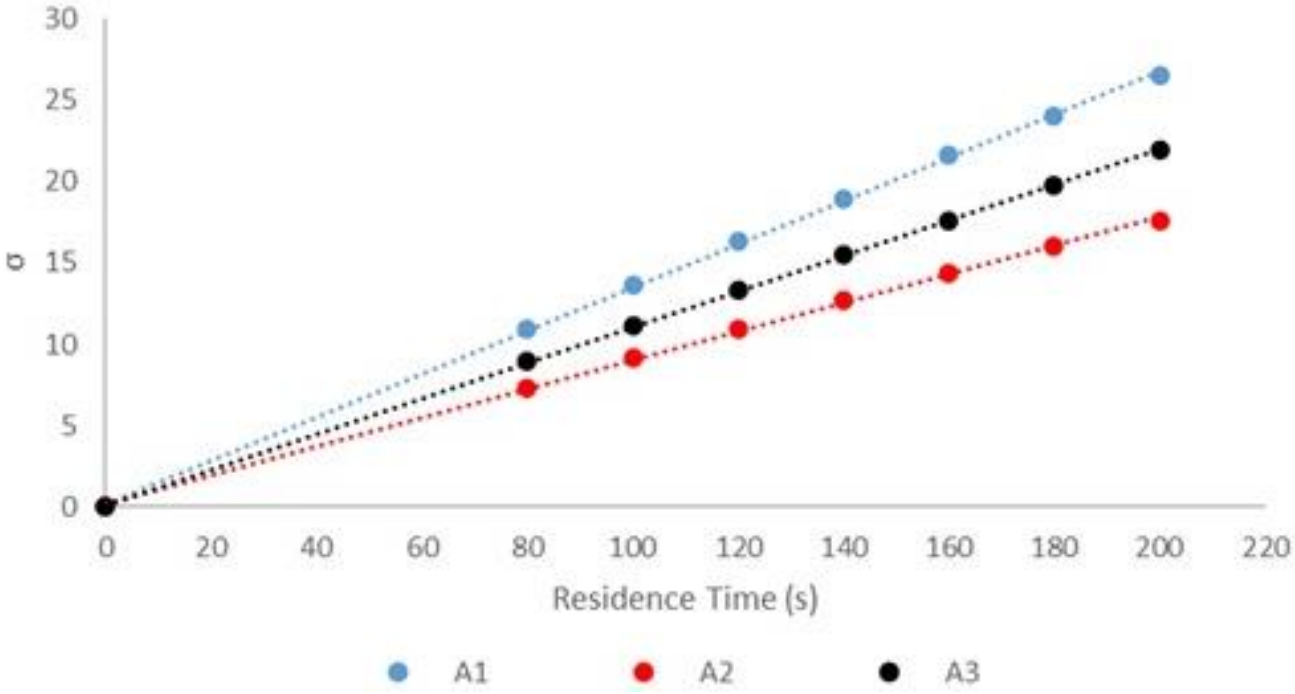

(**b**)

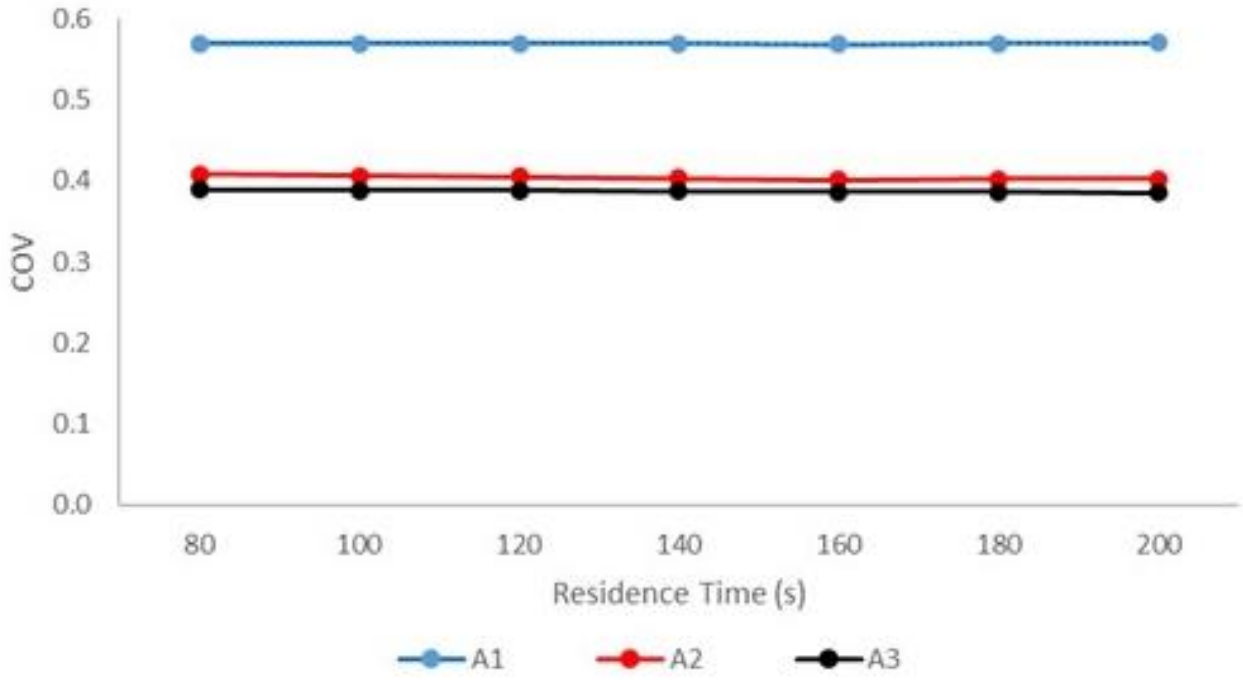

(**c**)

Figure 5. Trend of simulated temperature vs. residence time. (**a**) Mean temperature, (**b**) standard deviation and (**c**) COV.

Figure 5a highlights that in arrangement A3, after 150 s of treatment the final temperature exceeded 60 °C (goal of the design). The arrangements A1 and A2 had a similar temperature trend, but the temperature of 60 °C could only be reached after 200 s. Even if A3 had a standard deviation trend central to the other two conditions (see Figure 5b), it had the lowest trend of the COV, thus proving the configuration with better thermal uniformity (see Figure 5c). As a result, the A3 appears to be the most effective.

However, to check the thermal uniformity along the longitudinal axis, a second data processing step was carried out by dividing the whole length of the treatment chamber into three equal parts of 1 m each and grouping the 3D samples into three different subsets. The corresponding data are reported in Table 3.

Table 3. Simulated temperature at 1, 2 and 3 m lengths of treatment tube, versus the residence time.

Residence	1 m	2 m	3 m
Time [s]	$\mu \pm \Sigma$	$\mu \pm \sigma$	$\mu \pm \sigma$
		1 MW source 7.5 kW	
80	32.78 ± 7.46 b	42.83 ± 12.71 a	30.50 ± 7.10 b
100	36.87 ± 9.28 b	49.48 ± 15.81 a	34.08 ± 8.85 b
120	40.94 ± 11.09 b	56.11 ± 18.89 a	37.65 ± 10.60 b
140	45.02 ± 12.89 b	62.52 ± 22.09 a	41.18 ± 12.37 b
160	49.00 ± 14.65 b	69.32 ± 24.98 a	44.77 ± 14.08 b
180	52.55 ± 16.23 b	75.18 ± 27.69 a	47.92 ± 15.62 b
200	56.23 ± 17.85 b	81.26 ± 30.48 a	51.19 ± 17.22 b
		3 MW sources 2.5 kW	
80	32.27 ± 7.83 b	32.62 ± 2.55 b	37.61 ± 8.36 a
100	36.32 ± 9.72 b	36.74 ± 3.17 b	42.94 ± 10.40 a
120	40.37 ± 11.57 b	40.86 ± 3.78 b	48.26 ± 12.42 a
140	44.41 ± 13.40 b	44.97 ± 4.38 b	53.55 ± 14.43 a
160	48.44 ± 15.21 b	49.06 ± 4.98 b	58.82 ± 16.43 a
180	52.00 ± 16.79 b	52.66 ± 5.52 b	63.50 ± 18.23 a
200	55.71 ± 18.42 b	56.42 ± 6.08 b	68.36 ± 20.07 a
		5 MW sources 1.5 kW	
80	36.80 ± 8.80 a	39.05 ± 5.27 a	41.91 ± 10.47 a
100	41.96 ± 10.95 a	44.75 ± 6.55 a	48.27 ± 13.04 a
120	47.09 ± 13.08 a	50.43 ± 7.81 a	54.61 ± 15.59 a
140	52.22 ± 15.19 a	56.09 ± 9.05 a	60.92 ± 18.12 a
160	57.05 ± 17.09 a	61.48 ± 10.12 a	66.77 ± 20.32 a
180	62.41 ± 19.35 a	67.36 ± 11.50 a	73.47 ± 23.15 a
200	67.48 ± 21.40 a	72.96 ± 12.71 a	79.70 ± 25.64 a

Different letters in rows denotes significant statistical differences according to Tukey test ($p < 0.05$). μ—average temperature, σ—standard deviation.

A1 showed a significant increase in the temperature in the central section of the treatment chamber, while between the initial and final section there were no significant differences. Also, in A2, there was a significant increase in temperature in the final section near the plant outlet compared to the previous two. On the other hand, A3 showed a greater heating uniformity along the treatment chamber; in fact, no significant difference in temperature was found along the whole tube length. Figure 6 shows the different thermal behaviors for the three arrangements considered for the residence time of 140 s.

By an inspection of Figure 6a, it is clear a hot spot in the central zone of the treatment chamber, thus confirming that a single MW source is not able to ensure uniform temperature heating over the entire length. Moreover, by inspecting Figure 6b,c, an improvement in the heating uniformity, starting from A2 to A3, can be observed.

Therefore, numerical simulations identified the A3 as the optimal one since it ensures the best uniformity of microwave heating of the almonds. This result was used to develop and construct the MW-assisted prototype plant.

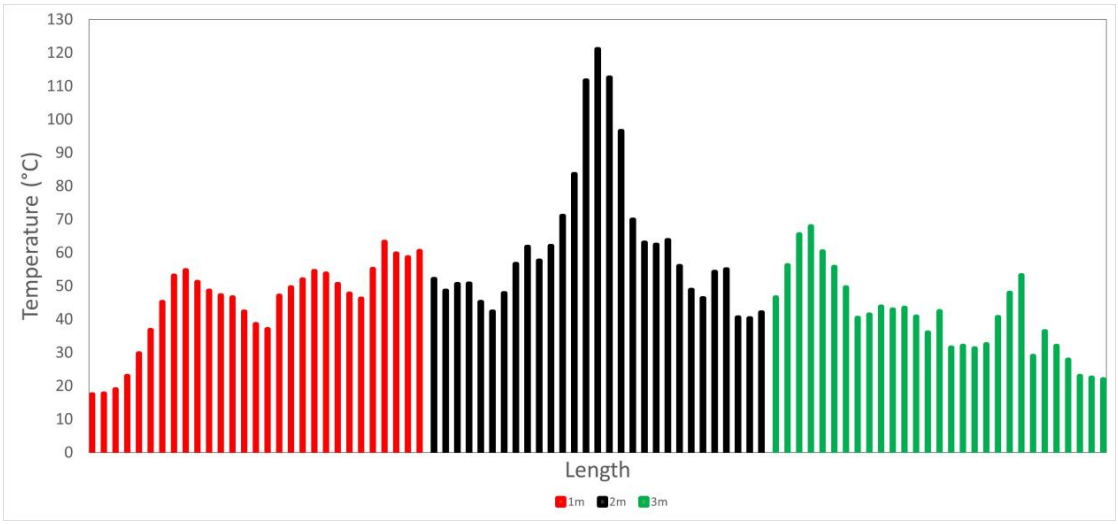

(**a**)

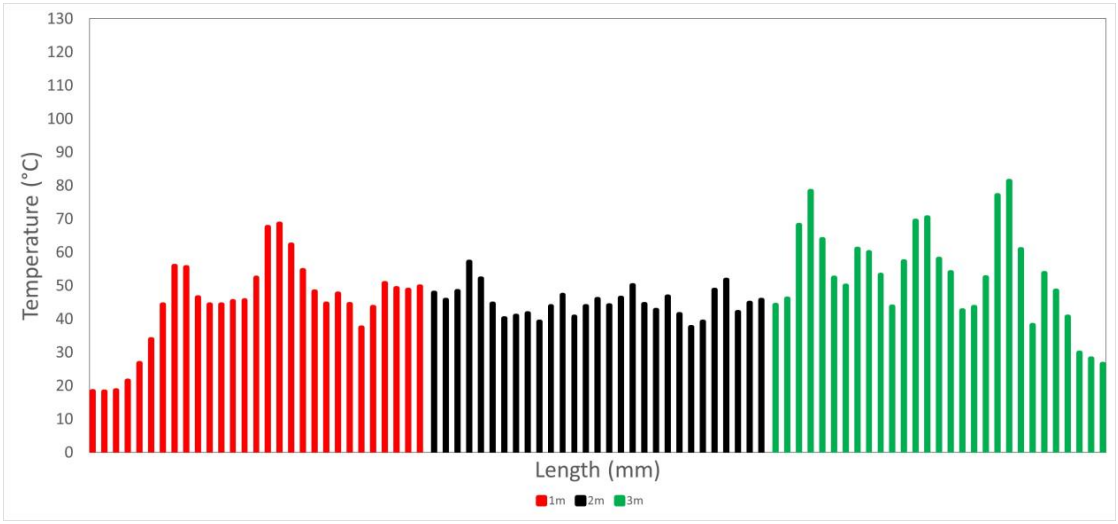

(**b**)

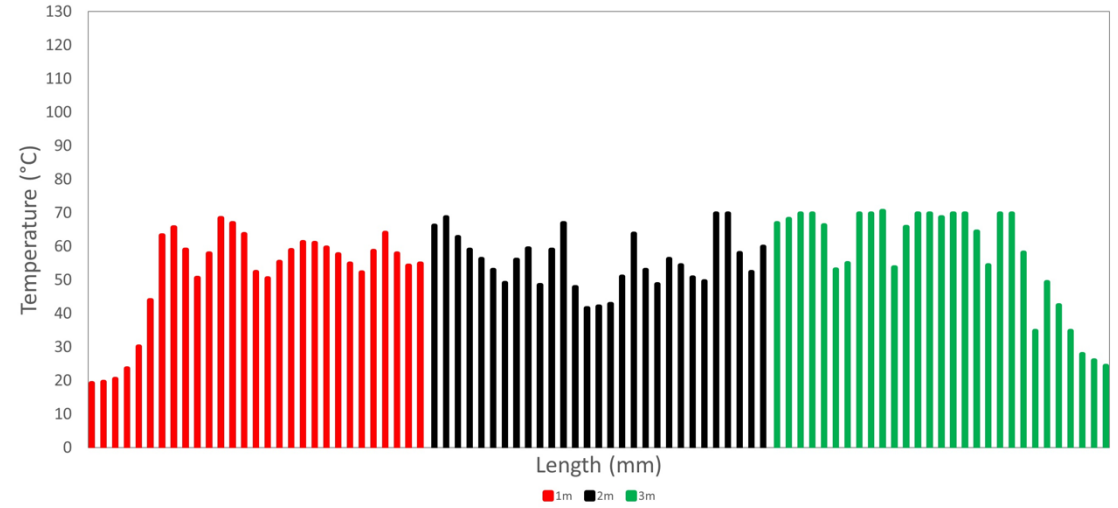

(**c**)

Figure 6. Trend of the simulated temperatures after 140 s of treatment for A1 (**a**), A2 (**b**) and A3 (**c**).

3.2. MW-Based Plant Prototype

According to the simulation evidence, the prototype was sized and designed with the aim of providing the continuous disinfestation of shelled almonds: a specific mass flow rate of at least 2 kg/min reaching 60 °C on the almonds' surface temperature after the treatment.

The prototype consisted of a shielded treatment chamber containing a polypropylene tube (length: 3000 mm; inner diameter: 90.8 mm) in which the almonds were irradiated by MW energy. A rotating metallic helix inside the tube allowed the almonds to pass easily from inlet to outlet. The rotating helix promoted constant mass mixing, providing a much more uniform distribution of the electromagnetic field for the almonds inside the treatment chamber. The helix was driven from an electric motor of 0.55 kW with reducer and integrated with variable frequency drive (VFD). The MW treatment chamber is a stainless steel reverberation chamber with an irregular shape to limit the possibility of stationary waves and hot spots. According to the numerical simulation carried out, the microwave power supply of the pilot plant consisted of five magnetron generators connected to the treatment chamber by standard WR340 rectangular waveguides. They operate at 2.45 GHz and can provide a variable output power up to a maximum of about 1.5 kW. They are equally spaced along the treatment chamber and each one is powered by a TM060 generator connected to a SM1180T power supply. The plant is equipped with a loading hopper of 40 L. The electric motor and magnetron generators can be turned on and off at different times. The process parameters, such as temperature, MW power, and speed, were constantly monitored using a PLC-based electronic control and management system.

Figure 7a shows the pilot plant prototype and Figure 7b a detail illustrating the magnetron generator (MW source) with the corresponding power supply, control, and cooling systems.

Figure 7. (**a**) MW-based plant prototype and (**b**) detail illustrating the magnetron generator, power supply, and control system.

3.3. Operative Parameters of MW-Based Plant Prototype

As reported in the previous section, the electric motor was equipped with a PLC-controlled VFD system to adjust motor frequency and the resulting helix rotation speed, the discharge speed (flow rate) and the residence time of the almonds in the treatment chamber. Figure 8 shows the trend of mass flow rate and the residence time as a function of motor frequencies. The increase in the engine motor frequency affects both the mass flow rate and the residence time, showing a nonlinear positive and negative relationship, respectively. At the minimum and maximum engine motor frequency, the mass flow rate varied from 1.9 to 5.4 kg/min and the residence time from 200 to 80 s, respectively, easily meeting the quantitative performance objectives set in the design step.

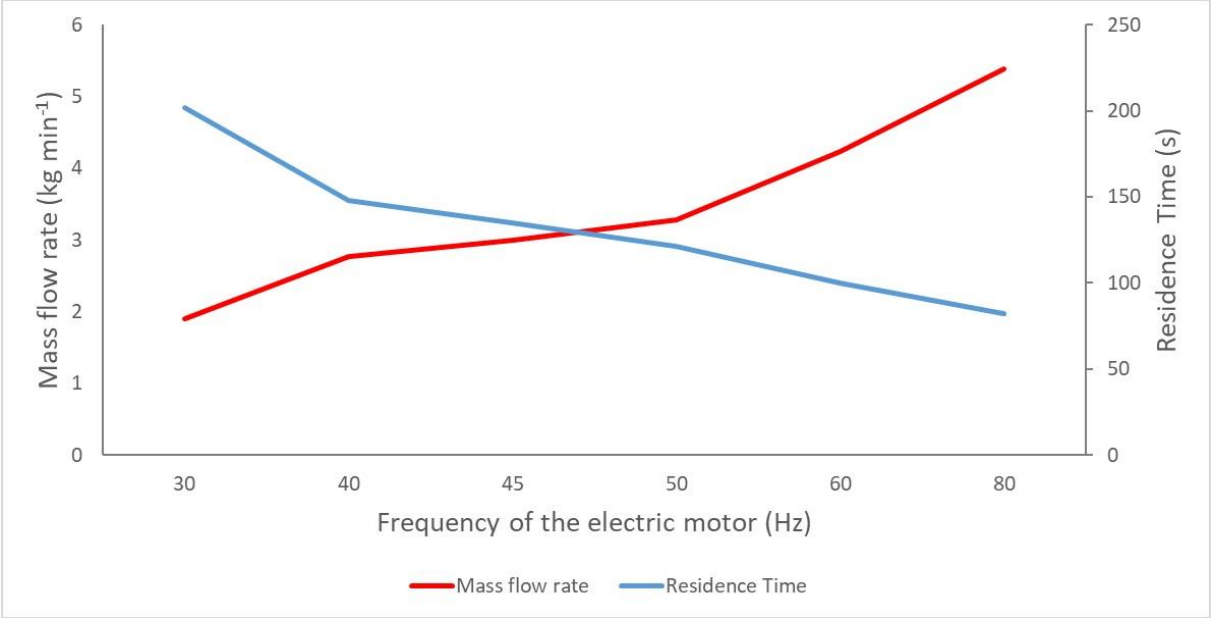

Figure 8. Mass flow rate and residence time versus the electric motor frequency.

Figure 9 shows the trend of the residence time versus the flow rate.

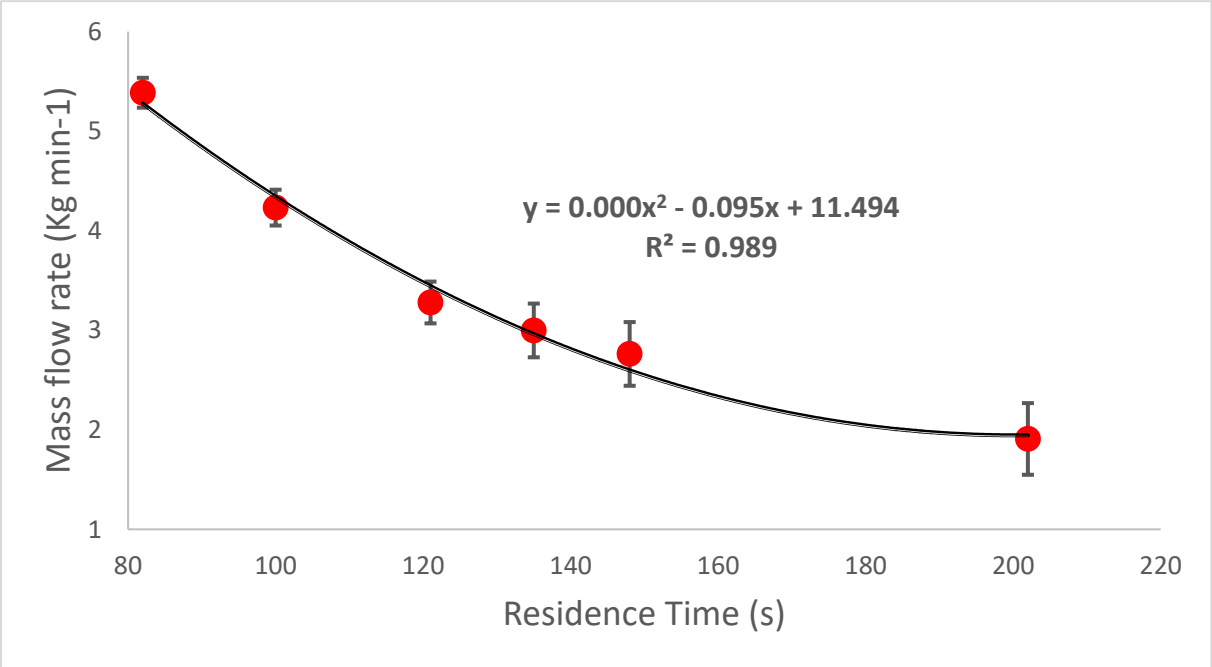

Figure 9. Trend of residence time versus mass flow rate.

A second-order polynomial regression was applied for all data points, obtaining an R-squared equal to 0.989.

As the frequency of the electric motor and the rotation speed of the helix inside the treatment tube increased, the residence time decreased, and the mass flow rate increased proportionally in the first half of the trend while in the second section it tended to saturate. This means that, although the helix inside the tube mixes the almonds well, the corresponding mass transport from the supply section to the discharge one does not occur with the same efficiency. In fact, once a certain rpm value of the helix has been exceeded, the almonds do not advance proportionally to the rotation speed of the helix.

3.4. Moisture Content

The results demonstrated that microwave treatment did not result in a significant change in moisture between untreated and microwave-treated almond samples.

In summary, we reported only the data of the untreated sample whose humidity was equal to 4.59 ± 0.55 and of the sample treated in the most severe condition (30 Hz and residence time of 200 s) whose humidity was equal to 4.23 ± 0.53. The differences found were not statistically significant ($p < 0.05$).

3.5. Model Verification

To verify the simulation results, the surface temperatures of almonds after microwave heating were measured using a thermal imager and compared with the simulation results.

In Table 4, the mean temperature (μ), standard deviation (SD) and both the simulated and experimental COV are summarized for each residence time.

Table 4. Simulated and experimental data of temperature of almond surfaces.

	Residence Time (s)							RMSE
	80	**100**	**120**	**140**	**160**	**180**	**200**	
μ rilevated	38.0	43.4	51.5	55.3	61.0	66.9	72.9	0.82
μ simulated	39.0	44.7	50.4	56.0	61.3	67.3	72.8	
σ rilevated	1.5	2.1	2.8	2.7	3.3	3.3	4.5	13.02
σ simulated	9.0	11.2	13.3	15.5	17.5	19.8	21.9	
COV rilevated	0.07	0.08	0.08	0.07	0.07	0.07	0.08	0.31
COV simulated	0.39	0.39	0.39	0.39	0.39	0.39	0.39	

The relationships between the mean temperature value, both simulated and experimental, are shown in Figure 10.

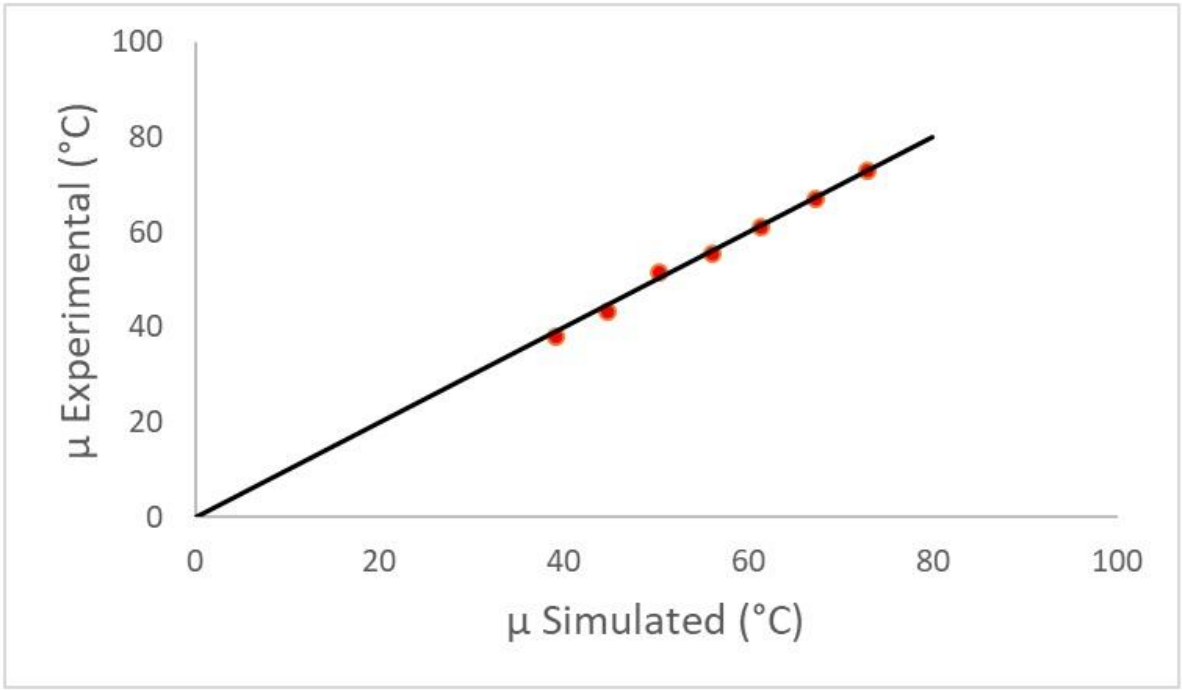

Figure 10. Comparison between simulated and experimental temperature values.

Figure 10 shows the comparison between the simulated and experimental temperature values. Considering the data shown in Table 4 and Figure 10, there was a perfect correspondence between the simulated and experimental values; this was also confirmed by the RMSE value; which was equal to 0.82. The results obtained prove that the numerical modeling can accurately predict the temperature trend.

The standard deviation for experimental data was much lower than the simulated one, consequentially leading to a high RMSE value (13.02), as shown in Table 4. This means that there is no good match between the simulated and measured standard deviations. However, between them a strong linear regression was detected (R^2 = 0.91), as shown in Figure 11. This means that even the standard deviation can be predicted.

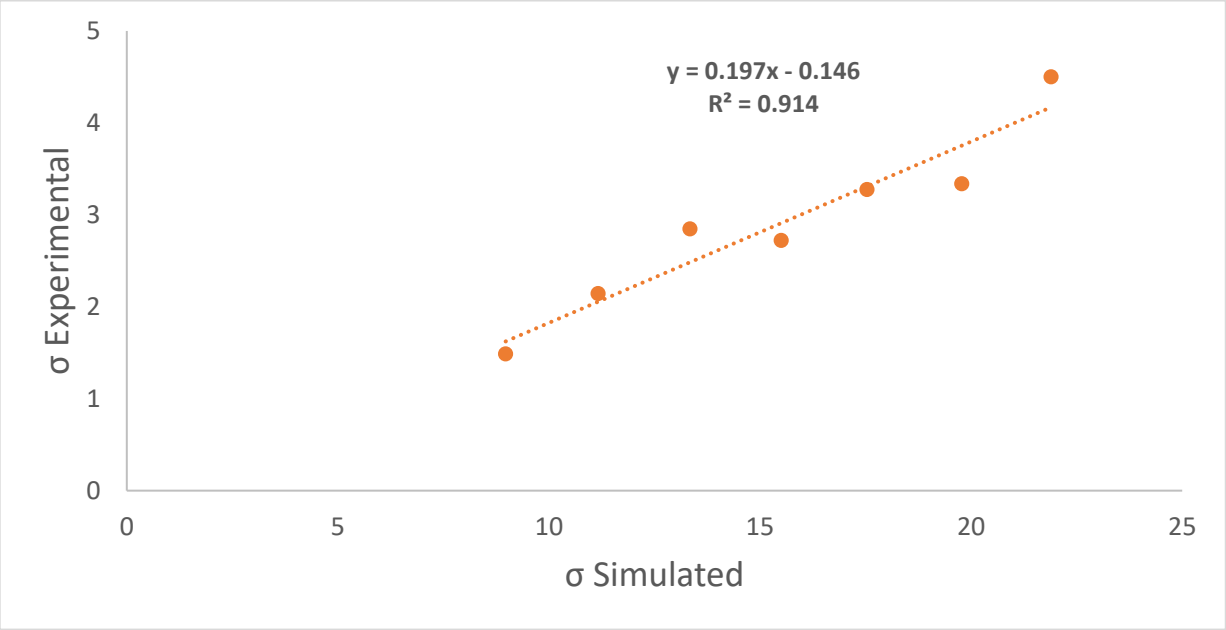

Figure 11. Simulated versus experimental temperature values.

It is important to remember that the numerical simulation was carried out in a static manner without considering the metal helix inserted in the treatment chamber. The helix has the function of transporting the almonds from the feed to the discharge, but also of mixing them. The lower standard deviation found during the experimental tests compared to that found in the numerical simulation confirms the effectiveness of the helix in mixing the almonds to guarantee their greater heating uniformity, as reported in [26,27].

In this study, the COV was used to evaluate the temperature uniformity of the outlet almond surface.

The COV for the experimental data ranged between 0.07 to 0.08 but it was also up to more than five times less than the simulated data. This occurrence confirms the efficient heating uniformity of the developed prototype, as also shown by the thermographic images (Figure 12).

Finally, the study demonstrated that the simulation results were in good agreement with the experimental findings and the operative process condition for almond disinfestation. With the help of the numerical simulation, the complex process of interaction between microwaves and almonds during the treatments was understood.

This study confirms that simulation is a powerful tool for the development of new technologies and above all for the investigation of heating uniformity, as also demonstrated in many other studies [33,46–50].

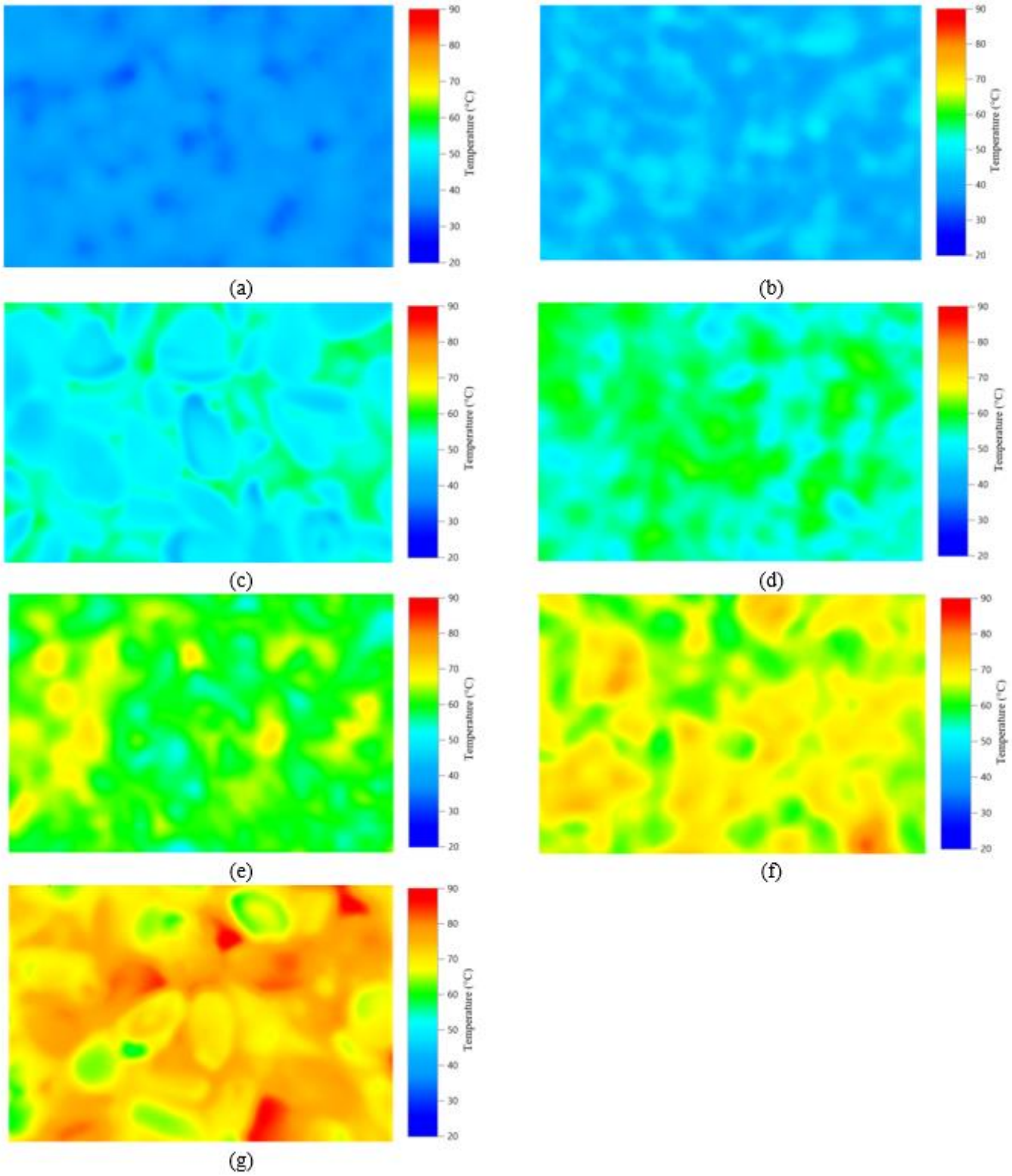

Figure 12. Thermal images of almonds after microwave heating for 80 s (**a**), 100 s (**b**), 120 s (**c**), 140 s (**d**), 160 s (**e**), 180 s (**f**) and 200 s (**g**).

4. Conclusions

This study presents the development of a continuous microwave (MW) prototype designed for the disinfestation of unshelled almonds, along with a numerical simulation aimed at optimizing the machine's design.

The developed prototype met all the objectives set regarding the minimum residence time of the almonds in the treatment chamber and the feeding flow rate.

The 3D Multiphysics model, which integrated electromagnetic and heat transfer processes, proved to be highly effective by yielding temperature values closely correlated with experimental data. Although the methodology used is accurate in calculating the average temperature, it did not provide useful information in predicting thermal uniformity indicators. However, a strong correlation was found between the simulated and experimental thermal uniformity.

Consequently, this model stands as a valuable tool for conducting a precise preventive analysis at the overall plant level, encompassing MW power, temperature distributions, residence times, and plant footprint. Notably, since there are a lack of studies on the treatment of shelled almonds using a continuous-flow microwave heating system, this study offers potential contributions to the design of microwave heating systems, contributing positively towards the use of physical rather than chemical methodologies for post-harvest disinfestation treatments.

Author Contributions: A.L., L.M. and A.T.: conceptualization, writing, review, and editing; A.B.: experimental test, figures, tables, and data analysis; C.M.L., A.F. and D.C.: experimental test and data analysis. All authors have read and agreed to the published version of the manuscript.

Funding: PSR Puglia 2014–2020, sottomisura 16.2, Progetto "Almond Management Innovations (Approcci per una Mandorlicoltura biologica)–AM'I", funded by "PSR Puglia 2014–2020, sottomisura 16.2–prog. AMI'—Grant number: B99J20000110009, D.d.S. n. 94250025148.

Institutional Review Board Statement: Not applicable.

Informed Consent Statement: Not applicable.

Data Availability Statement: The raw data supporting the conclusions of this article will be made available by the authors on request.

Conflicts of Interest: Author Claudio Maria Lamacchia, Angela Ferraris and Domenico Caggiano was employed by the company IAMAtek srl. The remaining authors declare that the research was conducted in the absence of any commercial or financial relationships that could be construed as a potential conflict of interest.

References

1. Yada, S.; Lapsley, K.; Huang, G. A review of composition studies of cultivated almonds: Macronutrients and micronutrients. *J. Food Compos. Anal.* **2011**, *24*, 469–480. [CrossRef]
2. Choo, J.M.; Tran, C.D.; Luscombe-Marsh, N.D.; Stonehouse, W.; Bowen, J.; Johnson, N.; Thompson, C.H.; Watson, E.-J.; Brinkworth, G.D.; Rogers, G.B. Almond consumption affects fecal microbiota composition, stool pH, and stool moisture in overweight and obese adults with elevated fasting blood glucose: A randomized controlled trial. *Nutr. Res.* **2021**, *85*, 47–59. [CrossRef]
3. Barreca, D.; Nabavi, S.M.; Sureda, A.; Rasekhian, M.; Raciti, R.; Silva, A.S.; Annunziata, G.; Arnone, A.; Tenore, G.C.; Süntar, İ.; et al. Almonds (*Prunus dulcis* Mill. D. A. Webb): A Source of Nutrients and Health-Promoting Compounds. *Nutrients* **2020**, *12*, 672. [CrossRef]
4. Bernat, N.; Cháfer, M.; Chiralt, A.; González-Martínez, C. Development of a non-dairy probiotic fermented product based on almond milk and inulin. *Food Sci. Technol. Int.* **2015**, *21*, 440–453. [CrossRef] [PubMed]
5. Gautam, C.; Islam, S.M.; Sadistap, S.; Sarma, U. Effect of Microwave Heat on the Nutritional Properties of Infected Red Kidney Beans. *IEEE Access* **2018**, *6*, 57137–57143. [CrossRef]
6. Yadav, D.N.; Anand, T.; Sharma, M.; Gupta, R.K. Microwave technology for disinfestation of cereals and pulses: An overview. *J. Food Sci. Technol.* **2014**, *51*, 3568–3576. [CrossRef]
7. Chenlo, F.; Moreira, R.; Chaguri, L.; Torres, M.D. Note. Sugar, moisture contents, and color of chestnuts during different storage regimes. *Food Sci. Technol. Int.* **2009**, *15*, 169–178. [CrossRef]
8. Wang, S.; Tiwari, G.; Jiao, S.; Johnson, J.; Tang, J. Developing postharvest disinfestation treatments for legumes using radio frequency energy. *Biosyst. Eng.* **2010**, *105*, 341–349. [CrossRef]
9. Kovács, E.; Kiss, I.; Boros, A.; Horváth, N.; Tóth, J.; Gyulai, P.; Szalma, Á. Disinfestation of different cereal products by irradiation. *Int. J. Radiat. Appl. Instrum. Part C Radiat. Phys. Chem.* **1986**, *28*, 545–548. [CrossRef]
10. Patil, H.; Shejale, K.P.; Jabaraj, R.; Shah, N.; Kumar, G. Disinfestation of red flour beetle (*Tribolium castaneum*) present in almonds (*Prunus dulcis*) using microwave heating and evaluation of quality and shelf life of almonds. *J. Stored Prod. Res.* **2020**, *87*, 101616. [CrossRef]

11. Gao, M.; Tang, J.; Wang, Y.; Powers, J.; Wang, S. Almond quality as influenced by radio frequency heat treatments for disinfestation. *Postharvest Biol. Technol.* **2010**, *58*, 225–231. [CrossRef]
12. Paul, A.; Radhakrishnan, M.; Anandakumar, S.; Shanmugasundaram, S.; Anandharamakrishnan, C. Disinfestation techniques for major cereals: A status report. *Compr. Rev. Food Sci. Food Saf.* **2020**, *19*, 1125–1155. [CrossRef] [PubMed]
13. Hou, L.; Ling, B.; Wang, S. Development of thermal treatment protocol for disinfesting chestnuts using radio frequency energy. *Postharvest Biol. Technol.* **2014**, *98*, 65–71. [CrossRef]
14. Wang, S.; Tang, J. Radio frequency and microwave alternative treatments for nut insect control: A review. *Agric. Eng. J.* **2001**, *10*, 105–120.
15. Manickavasagan, A.; Alahakoon PM, K.; Al-Busaidi, T.K.; Al-Adawi, S.; Al-Wahaibi, A.K.; Al-Raeesi, A.A.; Al-Yahyai, R.; Jayas, D.S. Disinfestation of stored dates using microwave energy. *J. Stored Prod. Res.* **2013**, *55*, 1–5. [CrossRef]
16. Gamage, T.V.; Sanguansri, P.; Swiergon, P.; Eelkema, M.; Wyatt, P.; Leach, P.; Alexander, D.L.J.; Knoerzer, K. Continuous combined microwave and hot air treatment of apples for fruit fly (*Bactrocera tryoni* and *B. jarvisi*) disinfestation. *Innov. Food Sci. Emerg. Technol.* **2015**, *29*, 261–270. [CrossRef]
17. Ipsita, D.; Narendra, G.S.; Girish, K. Properties of walnut influenced by short time microwave treatment for disinfestation of insect infestation. *J. Stored Prod. Res.* **2014**, *59*, 152–157.
18. Fuji, J.; Digvir, S.J.; Noel, D.G.W.; Fields, P.G.; Howe, N. An evaluation of insect expulsion from wheat samples by microwave treatment for disinfestation. *Biosyst. Eng.* **2015**, *130*, 1–12.
19. Candido da Silva, A.; Sarturi, H.J.; Dall'Oglio, E.L.; Soares, M.A.; de Sousa, P.T.; Gomes de Vasconcelos, L.; Kuhnen, C.A. Microwave drying and disinfestation of Brazil nut seeds. *Food Control* **2016**, *70*, 119–129. [CrossRef]
20. Wang, S.; Tang, J.; Cavalieri, R.P. Modeling fruit internal heating rates for hot air and hot water treatments. *Postharvest Biol. Technol.* **2001**, *22*, 257–270. [CrossRef]
21. Falciglia, P.P.; Roccaro, P.; Bonanno, L.; De Guidi, G.; Vagliasindi, F.G.A.; Romano, S. A review on the microwave heating as a sustainable technique for environmental remediation/detoxification applications. *Renew. Sustain. Energy Rev.* **2018**, *95*, 147–170. [CrossRef]
22. Liu, T.-C.; Wu, Y.-C.; Chau, C.-F. An Overview of Carbon Emission Mitigation in the Food Industry: Efforts, Challenges, and Opportunities. *Processes* **2023**, *11*, 1993. [CrossRef]
23. Shen, L.; Gao, M.; Feng, S.; Ma, W.; Zhang, Y.; Liu, C.; Liu, C.; Zheng, X. Analysis of heating uniformity considering microwave transmission in stacked bulk of granular materials on a turntable in microwave ovens. *J. Food Eng.* **2022**, *319*, 110903. [CrossRef]
24. Gallo, M.; Bozzetti, M.; Calo, G.; Mescia, L.; Petruzzelli, V. Design of a Dielectric Applicator for Microwave Heating. *J. Microw. Power Electromagn. Energy* **2009**, *43*, 4–12. [CrossRef] [PubMed]
25. Vadivambal, R.; Jayas, D.S. Non-uniform Temperature Distribution During Microwave Heating of Food Materials—A Review. *Food Bioprocess Technol.* **2010**, *3*, 161–171. [CrossRef]
26. Zhu, H.; Ye, J.; Gulati, T.; Yang, Y.; Liao, Y.; Yang, Y.; Huang, K. Dynamic analysis of continuous-flow microwave reactor with a screw propeller. *Appl. Therm. Eng.* **2017**, *123*, 1456–1461. [CrossRef]
27. Sebera, V.; Nasswettrová, A.; Nikl, K. Finite Element Analysis of Mode Stirrer Impact on Electric Field Uniformity in a Microwave Applicator. *Dry. Technol.* **2012**, *30*, 1388–1396. [CrossRef]
28. Birla, S.L.; Pitchai, K. 18—Simulation of microwave processes. In *The Microwave Processing of Foods*, 2nd ed.; Woodhead Publishing Series in Food Science, Technology and Nutrition; Regier, M., Knoerzer, K., Schubert, H., Eds.; Woodhead Publishing: Sawston, UK, 2017; pp. 407–431, ISBN 9780081005286. [CrossRef]
29. Yang, H.; Yan, B.; Meng, L.; Jiao, X.; Huang, J.; Gao, W.; Zhao, J.; Zhang, H.; Chen, W.; Fan, D. Mathematical modeling of continuous microwave heating of surimi paste. *J. Food Eng.* **2022**, *315*, 110797. [CrossRef]
30. Yang, H.; Yan, B.; Chen, W.; Fan, D. Prediction and innovation of sustainable continuous flow microwave processing based on numerical simulations: A systematic review. *Renew. Sustain. Energy Rev.* **2023**, *175*, 113183. [CrossRef]
31. Campañone, L.A.; Bava, J.A.; Mascheroni, R.H. Modeling and process simulation of controlled microwave heating of foods by using of the resonance phenomenon. *Appl. Therm. Eng.* **2014**, *73*, 914–923. [CrossRef]
32. Mescia, L.; Lamacchia, C.M.; Berardi, A.; Leone, A.; Tamborrino, A. Continuous microwave pilot plant for almond disinfestation: Preliminary tests. In Proceedings of the Microwave Mediterranean Symposium (MMS 2022), Pizzo Calabro, Italy, 9–13 May 2022. [CrossRef]
33. Tamborrino, A.; Berardi, A.; de Lillo, E.; Ragone, G.; De Benedictis, M.; Tufariello, M.; Santino, A.; Leone, A. Using a continuous microwave system for postharvest almond disinfestation. *Postharvest Biol. Technol.* **2023**, *201*, 112369. [CrossRef]
34. Tamborrino, A.; Summo, C.; Berardi, A.; De Angelis, D.; Ragone, G.; Leone, A. Use of a Microwave Pilot Plant for Almond Disinfestation: Study on the Thermal Uniformity of the Treatment and Effect on Volatile Composition. *Chem. Eng. Trans.* **2023**, *102*, 79–84. [CrossRef]
35. ICNIRP. Guidelines for limiting exposure to electromagnetic fields (100 kHz to 300 GHz). *Health Phys.* **2020**, *118*, 483–524. [CrossRef] [PubMed]
36. Directive 2013/35/EU of the European Parliament and of the Council of 26 June 2013 on the Minimum Health and Safety Requirements Regarding the Exposure of Workers to the Risks Arising from Physical Agents (Electromagnetic Fields) (20th Individual Directive within the Meaning of Article 16(1) of Directive 89/391/EEC) and Repealing Directive 2004/40/EC.

37. Legislative Decree No. 159 of August 1, 2016, Implementing EU Directive 2013/35/UE on the Minimum Safety and Health Standards Related to the Exposure of Workers to Risks Deriving from Physical Agents (Electromagnetic Fields) and Repealing EU Directive 2004/40/CE (L.D. No. 159), Gazetta Ufficiale, No. 192 (18 August 2016), NORMATTIVA. (In Italian)
38. Laneve, D.; Falconi, M.C.; Bozzetti, M.; Rutigliani, G.; Prisco, R.A.; Dimiccoli, V.; Prudenzano, F. Electromagnetic Design of Microwave Cavities for Side-Coupled Linear Accelerators: A Hybrid Numerical/Analytical Approach. *IEEE Trans. Nucl. Sci.* **2018**, *65*, 2233–2239. [CrossRef]
39. Nelson, S.O. *Dielectric Properties of Agricultural Materials and their Applications*; Academic Press: London, UK, 2015.
40. Weng, Y.-K.; Chen, J.; Cheng, C.-W.; Chen, C. Use of Modern Regression Analysis in the Dielectric Properties of Foods. *Foods* **2020**, *9*, 1472. [CrossRef] [PubMed]
41. Li, R.; Zhang, S.; Kou, X.; Ling, B.; Wang, S. Dielectric properties of almond kernels associated with radio frequency and microwave pasteurization. *Sci. Rep.* **2017**, *7*, srep42452. [CrossRef] [PubMed]
42. Collin, R.E. *Foundation of Microwave Engineering*, 2nd ed.; Wiley-IEEE Press: Hoboken, NJ, USA, 2000.
43. Hahn, D.W.; Ozisik, M.N. *Heat Conduction*, 3rd ed.; John Wiley & Sons: Hoboken, NJ, USA, 2012; pp. 6–16.
44. Mescia, L.; Bia, P.; Chiapperino, M.A.; Caratelli, D. Fractional Calculus Based FDTD Modeling of Layered Biological Media Exposure to Wideband Electromagnetic Pulses. *Electronics* **2017**, *6*, 106. [CrossRef]
45. *UNI EN ISO 18134–1:2015*; Solid Biofuels—Determination of Moisture Content—Oven Dry Method—Part 1: Total Moisture—Reference Method. ISO: Geneva, Switzerland, 2022.
46. Chen, H.; Tang, J.; Liu, F. Simulation model for moving food packages in microwave heating processes using conformal FDTD method. *J. Food Eng.* **2008**, *88*, 294–305. [CrossRef]
47. Resurreccion, F.; Tang, J.; Pedrow, P.; Cavalieri, R.; Liu, F.; Tang, Z. Development of a computer simulation model for processing food in a microwave assisted thermal sterilization (MATS) system. *J. Food Eng.* **2013**, *118*, 406–416. [CrossRef]
48. Kako, Y.; Llave, Y.; Sakai, N.; Fukuoka, M. Computer simulation of microwave cooking of sweet potato—Kinetics analysis of reactions in the maltose production process and their modeling. *J. Food Eng.* **2023**, *349*, 111469. [CrossRef]
49. Perone, C.; Romaniello, R.; Leone, A.; Berardi, A.; Catalano, P.; Tamborrino, A. CFD Analysis of a Tube-in-tube Heat Exchanger to Pre-heat Olive Pastes. *Chem. Eng. Trans.* **2021**, *87*, 253–258. [CrossRef]
50. Leone, A.; Perone, C.; Berardi, A.; Tamborrino, A. Energy analysis and numerical evaluation of the decanter centrifuge for wastewater management to allow a sustainable energy planning of the process. *Energy Convers. Manag. X* **2024**, *22*, 100596. [CrossRef]